scientific reports

OPEN

Facile synthesis of Fe$_2$O$_3$, Fe$_2$O$_3$@CuO and WO$_3$ nanoparticles: characterization, structure determination and evaluation of their biological activity

Asmaa T. Mohamed[1], Reda Abdel Hameed[2,3], Shahira H. EL-Moslamy[4], Mohamed Fareid[2,3], Mohamad Othman[2,3], Samah A. Loutfy[1,5], Elbadawy A. Kamoun[1,6,7✉] & Mohamed Elnouby[8✉]

Due to their high specific surface area and its characteristic's functionalized nanomaterials have great potential in medical applications specialty, as an anticancer. Herein, functional nanoparticles (NPs) based on iron oxide Fe$_2$O$_3$, iron oxide modified with copper oxide Fe$_2$O$_3$@CuO, and tungsten oxide WO$_3$ were facile synthesized for biomedical applications. The obtained nanomaterials have nanocrystal sizes of 35.5 nm for Fe$_2$O$_3$, 7 nm for Fe$_2$O$_3$@CuO, and 25.5 nm for WO$_3$. In addition to octahedral and square nanoplates for Fe$_2$O$_3$, and WO$_3$; respectively. Results revealed that Fe$_2$O$_3$, Fe$_2$O$_3$@CuO, and WO$_3$ NPs showed remarked anticancer effects versus a safe effect on normal cells through cytotoxicity test using MTT-assay. Notably, synthesized NPs $e.g.$ our result demonstrated that Fe$_2$O$_3$@CuO exhibited the lowest IC$_{50}$ value on the $MCF-7$ cancer cell line at about 8.876 μg/ml, compared to Fe$_2$O$_3$ was 12.87 μg/ml and WO$_3$ was 9.211 μg/ml which indicate that the modification NPs Fe$_2$O$_3$@CuO gave the highest antiproliferative effect against breast cancer. However, these NPs showed a safe mode toward the $Vero$ normal cell line, where IC$_{50}$ were monitored as 40.24 μg/ml for Fe$_2$O$_3$, 21.13 μg/ml for Fe$_2$O$_3$@CuO, and 25.41 μg/ml for WO$_3$ NPs. For further evidence. The antiviral activity using virucidal and viral adsorption mechanisms gave practiced effect by viral adsorption mechanism and prevented the virus from replicating inside the cells. Fe$_2$O$_3$@CuO and WO$_3$ NPs showed a complete reduction in the viral load synergistic effect of combinations between the tested two materials copper oxide instead of iron oxide alone. Interestingly, the antimicrobial efficiency of Fe$_2$O$_3$@CuO NPs, Fe$_2$O$_3$NPs, and WO$_3$NPs was evaluated using $E. coli$, $S. aureus$, and $C. albicans$ pathogens. The widest microbial inhibition zone ($ca.$ 38.45 mm) was observed with 250 mg/ml of WO$_3$ NPs against $E. coli$, whereas using 40 mg/ml of Fe$_2$O$_3$@CuO NPS could form microbial inhibition zone $ca.$ 32.86 mm against $S. aureus$. Nevertheless, $C. albicans$ was relatively resistant to all examined NPs.

[1]Nanotechnology Research Center (NTRC), The British University in Egypt, El-Shorouk City, Suez Desert Road, P.O. Box 43, Cairo 11837, Egypt. [2]Basic Science Department, Preparatory Year, University of Ha'il, 1560 Hail, Saudi Arabia. [3]Medical and Diagnostic Research Centre, University of Ha'il, 55473 Ha'il, Saudi Arabia. [4]Bioprocess Development Department, Genetic Engineering and Biotechnology Research Institute (GEBRI), City of Scientific Research and Technological Applications (SRTA-City), New Borg Al-Arab City 21934, Alexandria, Egypt. [5]Virology and Immunology Unit, Cancer Biology Department, National Cancer Institute (NCI), Cairo University, Fom El-Khalig 11796, Cairo, Egypt. [6]Department of Chemistry, College of Science, King Faisal University, 31982 Al-Ahsa, Saudi Arabia. [7]Polymeric Materials Research Department, Advanced Technology and New Materials Research Institute (ATNMRI), City of Scientific Research and Technological Applications, New Borg Al-Arab City 21934, Alexandria, Egypt. [8]Nanotechnology and Composite Materials Department, Advanced Technology and New Materials Research (ATNMRI), City of Scientific Research and Technological Applications (SRTA-City), New Borg Al-Arab City 21934, Alexandria, Egypt. ✉email: badawykamoun@yahoo.com; elbadawy.kamoun@bue.edu.eg; m_nano2050@yahoo.com

The superior biomedical activities of these nanostructures might be due to their unique features and accepted evaluations.

Novel nanomaterials and advanced nanotechnologies prompt the fast development of new protocols for biomedical applications. Ferric oxide, ferric oxide modified with copper oxide and tungsten oxide attracts great attention, due to their (biomedical application), another remarkable feature of ferric oxide and tungsten oxide nanoparticles is their selective toxicity to cancer cells, which opens the way for a new promising pathway for treatment[1]. Recently, there is an important aspect of magnetic nanoparticles in relation to biomedical applications through their biocompatibility and chemical stability which play a great role in the antiviral, antimicrobial, and anticancer effects[2]. The interaction of MNPs with the biological system has the possibility of the target drug delivery and cancer therapy through escaping from the Reticuloendothelial System (RES) which forms part of the immune system[3]. Increasing the time of circulation makes them more effective and preferable than the traditional ways of cancer therapy as chemotherapy[4,5]. enhances their accumulation at the tumor site rather than the free anticancer drug which causes severe side effects[6]. Recent studies have elucidated that MNPs induce cancer cell ablation[7] by induction of cell apoptosis with limited toxicity to normal cells[8], (DNA fragmentation and caspase activation are the main hallmarks of apoptosis) with other mechanisms such as nanoparticle-mediated necrosis and autophagy[9], which added advantage to the concept of the traditional ways of anticancer drugs[10]. Cancer is a critical disease that scientists are interested in since it has a long history of being one of the major causes of mortality. Cancer is not a single condition; rather, it is a group of disorders characterized by unregulated cell development. Tumors are a severe risk of lethal disease that has no geographic or organ limits; they cause an annual global mortality of more than 12.7 million people. Tumor illnesses are often caused by mutations in genes that regulate growth and are involved in DNA repair, cell division, and death.

Iron oxide (Fe$_2$O$_3$) magnetic nanoparticles have many roles in biomedical applications; their chemical stability, biocompatibility, and size as nanoscales can be used as targeted therapy, cell leveling, repairing tissue, and hyperthermia[11] in addition to their anticancer, antibacterial, and antiviral mechanisms[12]. These nanoparticles' exceptional ability to trace and then eliminate cancer cell potentials ensures their uniqueness. Heating systems that rely on Fe3O4 to control the release of medications from their delivery system can also be used[13]. These systems are designed to release their substance at temperatures, which highlights further benefits of using the NPs-dependent delivery method in conjunction with the hyperthermia modality for cancer treatment. clinical diagnosis as magnetic fluid hyperthermia[14] (MFH) and their magnetic resonance image (MRI)[11]. Furthermore, their ability to interact with biological factors (*e.g.* virus, pathogen[1], or other biological targets and increase their signal sensitivity[15] with particular resolution[16] so, can be visualized by MRI and MFH[16,17]. Therefore, MNPs have attracted continuous attention due to highly functionalized magnetic nanoparticles[18] which are able not only to target cancer cells via selective interaction between nanoparticles and cancer cells, especially the tumor mass, but also via their utilization for tumor imaging as a diagnostic approach[7]. Iron oxide nanoparticles were found to make induction of reactive oxygen species (ROS), induce depletion of glutathione[19] further, reduce the matrix metalloproteinase-2 (MMP-2), loss of mitochondrial membrane potential[20,4], and activation of caspase-3 which is responsible for cell apoptosis[8,21]. Fe$_2$O$_3$ NPs were later used as a targeted therapy to reach the tumor mass directly through the bloodstream[3,22] with a compatible medium that can be dispersed in the form of clusters to prevent their aggregation[18,23]. Moreover, in parallel, MNPs were used as antiviral agents not only to prevent viral infection but also in clinical diagnosis for identifying the virus target[17]. This approach is based on targeting the virus through functionalized nanoparticles, hence preventing its pathogenesis by inhibiting or competing for its attachment to the host cells' receptors[24].

Iron oxide modified with copper oxide NPs plays a great role in biological applications, due to their biocompatibility with normal cells and affinity to express their effect on pathogenic cells[25], copper oxide nanoparticles have an effective role in inducing the anticancer effect of iron oxide nanoparticles through the production of reactive oxygen species (ROS)[26], lipid peroxidation and genotoxic effect by chromosomal damage[27] which pushes the cells to the apoptotic pathway in order to achieve tumor mass ablation[27,28]. Copper oxide nanoparticles showed a higher apoptotic effect[29] and antimetastatic potential[30] which was accomplished by elevating the cellular reactive species[31], inhibiting of matrix metallopeptidase 9, and enhancing P53 expression which increases the apoptotic pathway[32,33]. Which assists the anticancer activity of iron oxide nanoparticles.

The antimicrobial effect of copper oxide NPs was determined by releasing Cu^{2+} ions leading to ROS production[34] and interacting directly with bacterial cells through the cell membrane of a biological target thus, exerting its bactericidal effect[34].

Tungsten oxide (WO$_3$) NPs have a characteristic scale and feature role to be used as an anticancer agent through cell membrane damage, denaturation to proteins, and ROS production with ultimate apoptosis and cell death[35,36]. So, WO$_3$ NPs have genotoxic and cytotoxic effects through their interference with DNA and protein of DNA synthesis or attacking the 5th phosphate group of DNA. And already expressed their genotoxic effect through oxidative stress by the production of ROS[37], thus leading to damage to the lipid and cell membrane[38,39]. Furthermore, WO$_3$ NPs have antimicrobial effects[40] by interacting with the bacterial cell membrane[39], followed by the destruction of the bacterial cell[41,42]. Additionally, MNPs have great virucidal activity against human Adenovirus type-5 (HAdV-5)[43]. The ability of the MNPs to block the viral cell surface receptor, prevent viral attachment and viral entry to the cells, and preventing its pathogenesis through. Which, it makes irreversible changes inside the viral genome[42], meanwhile prevent its replication inside the treated cells[44,45]. The magnetic nanoparticles (MNPs) might be functionalized intensively for great benefits in biomedical applications. However,

MNPs like Fe_2O_3, Fe_2O_3@CuO, and WO_3 have not been entirely investigated lately regarding their biological activity evaluations in literature. Herein, this work aims to discuss simple synthesis routes, instrumental characterization, and biological activity evaluations of synthesized MNPs cytotoxicity, antimicrobial, and antiviral activities were assessed and discussed in detail. Our findings clarified the following potential mechanisms for this complex's impact on the used cell lines and explained the efficiency of the synergetic effect between iron oxide with copper oxide.

Materials and methods
Materials
Nanoparticles preparations
Iron metal powder (> 99%), copper nitrate (> 99%), and NaOH (> 99%) were purchased from Belaqmi Fine Chemicals, India, sodium tungstate ($Na_2WO_4\cdot2H_2O$, > 98%) was obtained from Sisco, India, ion-exchange resin (Rohm& Haas, France).

Cell culture: Vero cell line (normal monkey kidney cells), *MCF-7* cell line (breast cancer cells) was obtained from (Vaccination and Sera Collection Organization (VACSERA), Agouza, Giza, Egypt). Dulbecco's Modified Eagle Medium basal medium (DMEM) was purchased from (Sigma, Munich, Germany). And supplemented with 10% fetal bovine serum (FBS),1% penicillin–streptomycin (100 IU/ml), 1% L-glutamine, and 3% sodium bicarbonate were purchased from (Gibco, Merelbeke, Belgium). Trypsin–EDTA (0.025% trypsin and 0.0025% EDTA) and PBS (phosphate buffer saline) tablets were purchased from (Fisher Scientific, Loughborough, UK). MTT 3-(4,5-dimethylthiazol-2-yl)-2,5-diphenyltetrazolium bromide was purchased from (SERVA Electrophoresis GmbH, Heidelberg, Germany). Antimicrobial activity was tested using a variety of human pathogens, including *Gram*-negative bacteria (*Escherichia coli*), *Gram*-positive bacteria (*Staphylococcus aureus*), and fungal cells (*Candida albicans*). The tested human pathogens were kindly provided from GEBRI, SRTA-City, Alexandria, Egypt.

Synthesis of Fe_2O_3, Fe_2O_3@CuO and WO_3 NPs
Magnetic Fe_2O_3 NPs were prepared via a one-pot hydrothermal reaction method as described elsewhere[45]. Typically, 4 g of iron metal powder was mixed with 10 g of NaOH in 40 mL of distilled water for 10 min at room temperature. The mixture was transferred into a Teflon-lined steel autoclave container and aged in an oven at 120 °C for 24 h. The obtained powder was washed several times with distilled water and dried overnight at 60°C (Scheme 1).

Cu-doped Fe_2O_3 (Fe_2O_3@CuO NPs) were prepared via one put hydrothermal reaction method as described elsewhere[45]. 4 g of iron metal powder was mixed with 10 g of NaOH in 40 ml of 0.1 M copper nitrate solution, where the water mixture was kept under harsh stirring for 10 min at ambient conditions. The mixture was transferred into a Teflon-lined steel autoclave container and aged in an oven at 120 °C for 24 h. The obtained powder was washed several times with distilled water and dried overnight at 60 °C.

Tungsten oxide (WO_3 NPs) was synthesized as a previously reported method[45]. Briefly, 0.5 M Na_2WO_4 solution was prepared as described elsewhere as follows[45]: Sodium tungstate dihydrate ($Na_2WO_4\cdot2H_2O$, > 98%, Sisco, India) was dissolved in deionized milli-Q water. A column was packed with 30 ml of ion-exchange resin (Rohm& Haas, France). This column was washed several times with water before use. 10 ml of the (0.5 M Na_2WO_4) solution was loaded onto the column, to form yellowish and transparent tungstic acid (H_2WO_4) solution. The
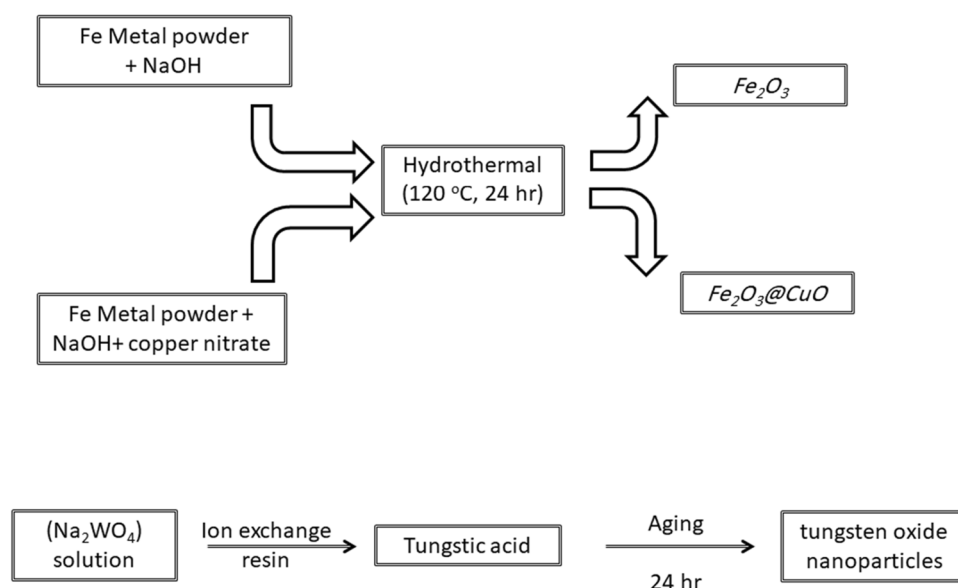
Scheme 1. Schematic diagram showing in brief the synthesis procedure of Fe_2O_3, Fe_2O_3@CuO and WO_3 NPs.

obtained solution was aged at room temperature for 24 h to produce precipitated tungsten oxide nanoparticles (Scheme 1).

Characterization

The synthesized nanoparticles were characterized by several characterization tools. Scanning electron microscopy (SEM, JEOL, JSM-6360LA, Japan) was used to investigate the morphological structure of the obtained materials[46]. The crystallographic phases of the produced samples were determined by X-ray powder diffraction (XRD, Shimadzu-7000, Japan)[47]. Fourier transform infrared (FTIR) was used to perform the chemical structure of all compounds by A Bruker ALPHA spectrometer (Bruker Corporation, Rheinstetten, Germany).

Biological activity evaluation

Antimicrobial activity

The antimicrobial activities of Fe_2O_3, $Fe_2O_3@CuO$, and WO_3 NPs were determined using the well-diffusion method as previously reported[48–50]. The bacteria and yeast cultures were grown in Luria–Bertani broth (0.5% yeast extract, 1% NaCl, and 1% tryptone) and Sabouraud dextrose broth (4% dextrose, 0.5% peptic digest of animal tissue, and 5% pancreatic digest of casein), respectively. The bacteria (10^6 bacteria/ml) and yeast (10^4 yeast/ml) were inoculated into 1% of the appropriate agar medium. After thoroughly shaking, 25 ml of the medium was transferred to sterile Petri plates (9 cm in diameter) and homogeneously distributed. Using a crock borer (6 mm in diameter), the wells were made into microbe agar plates[51]. The inhibitory concentration ranges were then determined by adding different concentrations of Fe_2O_3, $Fe_2O_3@CuO$, and WO_3 NPs (10, 50, 90, 130, 170, 210, 250, and 290 mg/ml) into these wells. Following that, varied concentrations of Fe_2O_3 NPs (5, 10, 15, and 20 mg/ml), $Fe_2O_3@CuO$ NPs (10, 20, 30, and 40 mg/ml), and WO_3 NPs (100, 150, 200, and 200 mg/ml) were loaded into the wells to determine the minimal inhibitory concentrations (MICs). Additionally, common antibiotics including 10 mg Ampicillin, 10 μg Penicillin, and 5 μg Ciprofloxacin discs were also surveyed as controls. The Petri dishes were then kept at 40 °C for an hour to allow the diffusion process to take place[52]. Then, the bacteria were incubated for 24 h at 37 °C and the yeasts for 72 h at 28 °C. Finally, the diameter of the created inhibitory zones on these plates was measured with a ruler (mm). After three repetitions of these experiments, average inhibition zones and their standard deviation values (mm ± SD) were calculated[53].

MTT assay

Cytoxicity of our synthesized NPS was determined by using MTT assay on *Vero* and *MCF-7* as normal models and human breast cancer cell lines, respectively[54]. Cells were seeded into a 96-well tissue culture plate with a density of ($2×10^4$) cells/ml and then, incubated at ambient conditions (37 °C, 5% CO_2, and humidity of 85–95%) for 24 h until reached complete sheet[55]. Afterward, cells were treated with synthesized NPs (Fe_2O_3, $Fe_2O_3@CuO$, and WO3 NPS) with concentrations (100, 50, 25, 12.5, 6.25, 3.125 μg/ml) for 48 h. Cell viability (%) was determined by applying MTT dye for 4 h then, 100 μl of DMSO was added to dissolve the formed crystals. The OD was measured at 570 nm using a microplate reader (CLARIOstar Plus, BMG LABTECH, Germany)[56,57].

$$Cell\ viability\ (\%) = \frac{Mean\ OD\ (S)}{Mean\ OD\ (C)} \times 100 \qquad (1)$$

Where OD (S) is the mean optical density of the tested sample and OD (C) refers to the mean optical density of the control group[58]. The relative cell viability % was plotted against the concentrations of the prepared NPs using *GraphPad Prism Version 6*.

Antiviral assay against human adenovirus type 5 (ADV-5)

<u>Virucidal mechanism.</u> *Vero* cells were seeded into a 6-well tissue culture plate with a density of ($5 × 10^5$ cells/well) till reached 90% confluency after 24 h incubation. Then, the cells were treated with synthesized materials (Fe_2O_3, $Fe_2O_3@CuO$, and WO_3 NPs) after their incubation at 4 °C for 1 h with 100 TCID50 of ADV load[59]. This procedure is based on the ability of the tested material to interact with the virus preventing its ability to replicate inside the host cells[60,61]. Then, viral copies were quantified by quantitative real-time PCR (RT-PCR)[62].

<u>Viral adsorption mechanism.</u> The viral adsorption mechanism was done via seeding *Vero* cells into a 6-well tissue culture plate at a density of ($5×10^5$) cells/well, then incubated for 24 h at ambient conditions. Upon reaching a confluency of > 90%, cells were treated with the tested NPs, then incubated for another 24 h. On the third day[63], the cells were infected with 100 TCID50 of the virus until the appearance of cytopathogenic effect (CPE)[64]. Finally, viral load was determined by quantitative RT-PCR[60,65]. The mechanism relies on the ability of tested material to inhibit viral entry into cells.

Statistical analysis

The obtained data were statically analyzed using an unpaired t-test with GraphPad Prism. The values were presented as the mean ± SD.

Ethics approval and consent to participate

Manuscripts report no studies involving human participants, human data, or human tissue. All experiments were performed in accordance with the Guidelines of the World Medical Association Declaration of Helsinki: Ethical Principles for Medical Research Involving Human Subjects and approved by the ethics committee at Cairo University and The British University in Egypt (BUE).

Results and discussion
Crystal structures investigation by XRD analysis

Figure 1 shows the XRD patterns of all synthesized magnetic nanoparticles (*i.e.* Fe_2O_3, Fe_2O_3@CuO, and WO_3 MNPs). XRD patterns show a single-phase structure of formed Fe_2O_3; while all peaks were indexed to the cubic Fe_3O_4 with a space group of Fd-3m (227) and lattice parameters: 8.3560 Å (ICDD Card No. 01-078-6916) (Fig. 1a).

Figure 1b shows the XRD pattern of synthesized Cu doped-MNPs. XRD pattern of Fe_2O_3@CuO shows a dual phase; where all peaks were indexed to the cubic Fe_3O_4 with a space group of Fd-3m (227) and lattice parameters: 8.3560 Å (*ICDD Card No. 01-078-6916*) and monoclinic CuO with a space group of C2/c (15) and lattice parameters: a ~ 4.7940 Å, b ~ 3.3620 Å, c ~ 5.2280 Å (*ICDD Card No. 01-076-7800*) (Fig. 1b). The obtained pattern is further evidencing the formation of dual phase between CuO doped onto Fe_2O_3.

Figure 1c shows the XRD pattern of synthesized tungsten oxide nanoparticles (WO_3 NPs). XRD pattern of tungsten oxide nanoparticles show a single phase, where all peaks were indexed to the orthorhombic $WO_3 \cdot H_2O$ with a space group of Pmnb (62) and lattice parameters: a ~ 5.2477 Å, b ~ 10.7851 Å, c ~ 5.1440 Å (*ICDD Card No. 00-018-1418*). The obtained patterns of WO_3 NPs are fully consistent with the previously published findings of Elnouby et al.[45].

The crystal sizes of the obtained nanoparticles were calculated from Debye-Scherer equation[42]:

$$D = \frac{K\lambda}{\beta \cos\theta} \tag{2}$$

where λ = 0.1542 nm is the Cu-K_α wavelength, K is a constant and is the FWHM.

Table 1 summarizes the crystal sizes of the obtained materials. It is noticeable that all obtained materials are in nanoscale size. Pure octahedral MNP has a crystal size of 35 nm, and by adding Copper the crystal size decreased to 7 nm coinciding with the disappearance of octahedral structure (Fig. 3). While tungsten oxide platelets have a lateral dimension of 33 nm and thickness of 25 nm.
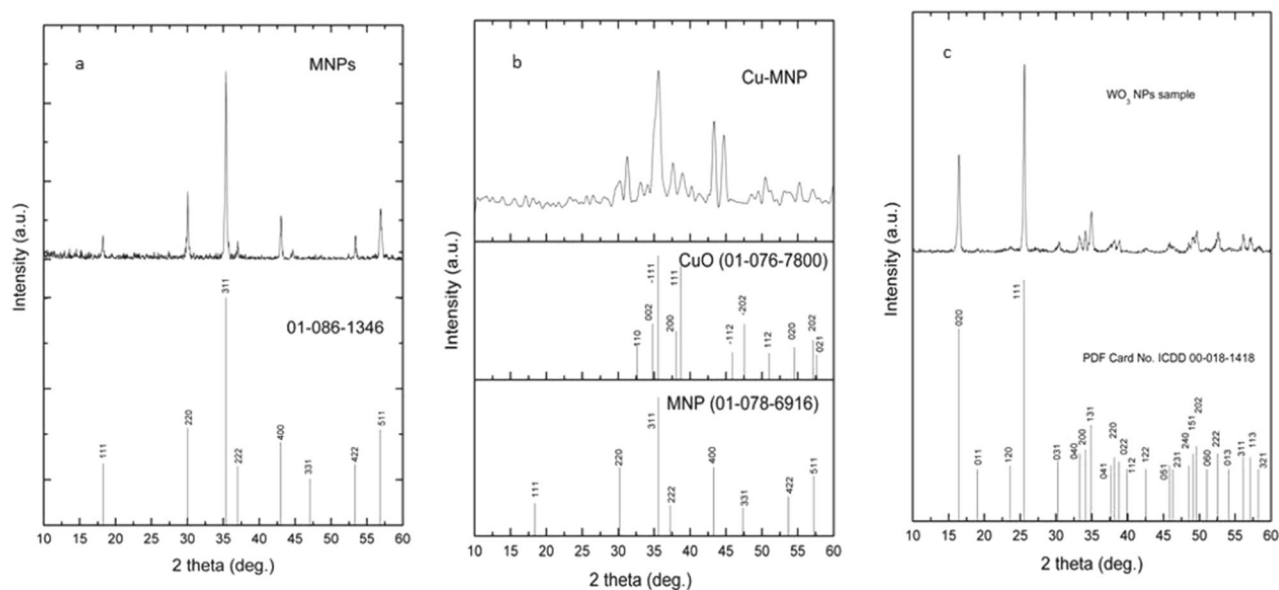

Figure 1. XRD pattern of synthesized magnetic NPs and their matched patterns as Fe_2O_3, Fe_2O_3@CuO and WO_3 (**a–c**); respectively.

Sample type	2Θ	Plane	Size (nm)
Fe_2O_3	35.37	311	35.5
Fe_2O_3@CuO	35.61	MNP (311) Cu (-111)	7
WO_3	25.61	111	33.5
	16.45	020	25.5

Table 1. Crystal sizes of the obtained synthesized materials.

FT-IR analysis

Figure 2 shows FTIR spectra of all synthesized Fe_2O_3, $Fe_2O_3@CuO$, and WO_3 MNPs. It was observed that the FTIR spectrum of Fe_2O_3 shows characteristics peaks at ν 3406 cm^{-1} revealing the stretching motion of (O–H) and the medium narrow band at ν 1616 cm^{-1}, characteristic of in-plane bending of (H–O-H) of the water molecule. Very intense broadband in the region at ν 902–621 cm^{-1} corresponds to different motions arising from W–O linkage[66]. Therefore, the band at ν 902 cm^{-1} refers to stretching ($W = O_t$) (where O_t is the terminal oxygen). While the bands at ν 763 and 694 cm^{-1} revealed the stretching (W–O) and the band at ν 713 cm^{-1} is due to stretching (W–O-W)[67]. On the other hand, the FTIR spectrum of synthesized Fe_2O_3 MNPs shows characteristic peaks also at the broadband at around 624–425 cm^{-1} revealing the vibrations of the Fe–O bonds of the magnetite[68].

Similarly, the FTIR spectrum of prepared Cu-doped MNP shows characteristic peaks at ν 525 cm^{-1} revealing the bending vibration of the Cu–O bond[69]. Briefly, all synthesized magnetic metal oxides (*i.e.* Fe_2O_3, $Fe_2O_3@$ CuO, and WO_3 MNPs) were characterized by a broad band around at ν 500 cm^{-1} indicating different modes of bending vibration of the metal–O bond. In addition, a few individual characteristic peaks are presented, where these peaks result from the crystal structures of nanoparticles, which play a definite role in their performance.

SEM investigation

Figure 3 shows the SEM surface investigation of all synthesized MNPs at two original magnifications. It was observed that Fe_2O_3 MNPs have a uniform octahedral structure and size. After adding CuO into Fe_2O_3MNPs, it lost its uniform octahedral structure, leading to forming of a homogeneously coated bilayer structure that uniformly distributed on the surface of the Fe_2O_3 MNPs. Notably, an SEM micrograph revealed that WO_3 NPs composed of a large number of square nano-plates. In addition, the average particle size of Fe_2O_3 and WO_3 NPS was measured from SEM micrographs. Size distribution histograms were listed supplementary in Fig. S1 (*supplementary data*). The average size of octahedral MNPs was 1.5 ~ 2.0 μm. However, the lateral dimension of the WO_3 nano-plates reached several hundreds of nanometers.
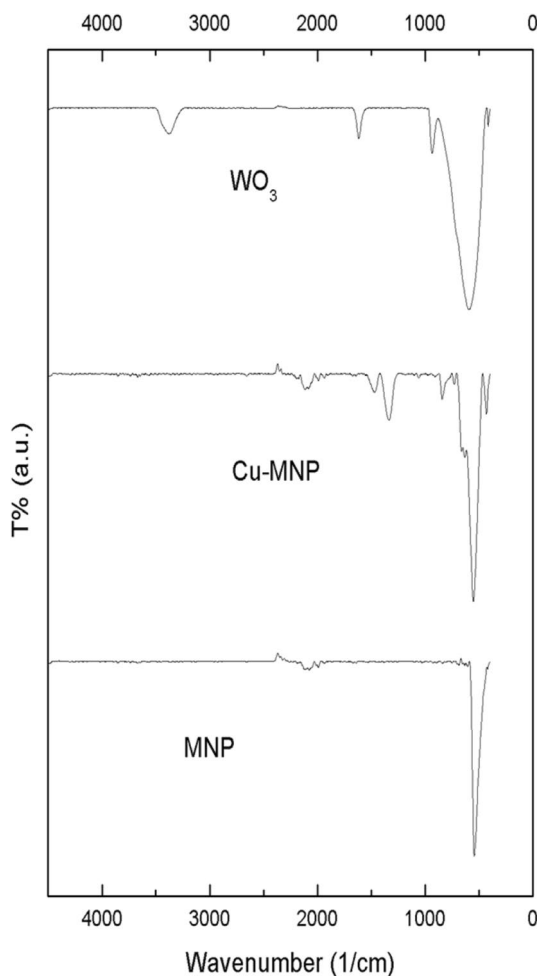

Figure 2. FT-IR spectra of synthesized magnetic NPs as Fe_2O_3, $Fe_2O_3@CuO$ and WO_3 (down-to-up); respectively.

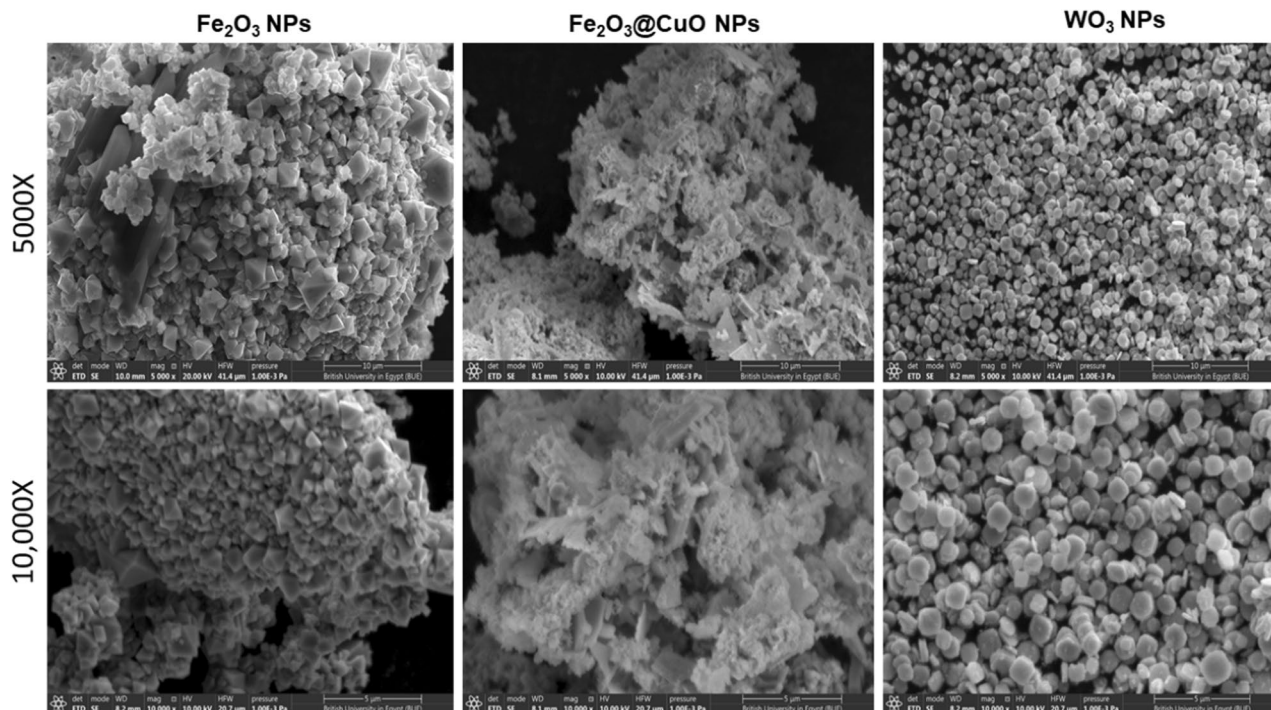**Figure 3.** SEM micrographs of synthesized magnetic NPs of Fe_2O_3, Fe_2O_3@CuO and WO_3, where all images were taken at (original magnification 5000X and 10,000X, scale 10 and 5 μm and applied voltage at 20 kV).

EDAX analysis

The compositional and elemental analysis of all synthesized MNPs was examined and verified using an EDAX-SEM unit and shown in Fig. 4. The composition of Fe_2O_3, Fe_2O_3@CuO, and WO_3 NPs were (Fe, O), (Fe, O, Cu), and (W, O); respectively, which indicate that no contaminated elements were detected for all samples. In additions, the composition ratios in all provided samples confirmed its compositions- as listed in Table 2 from
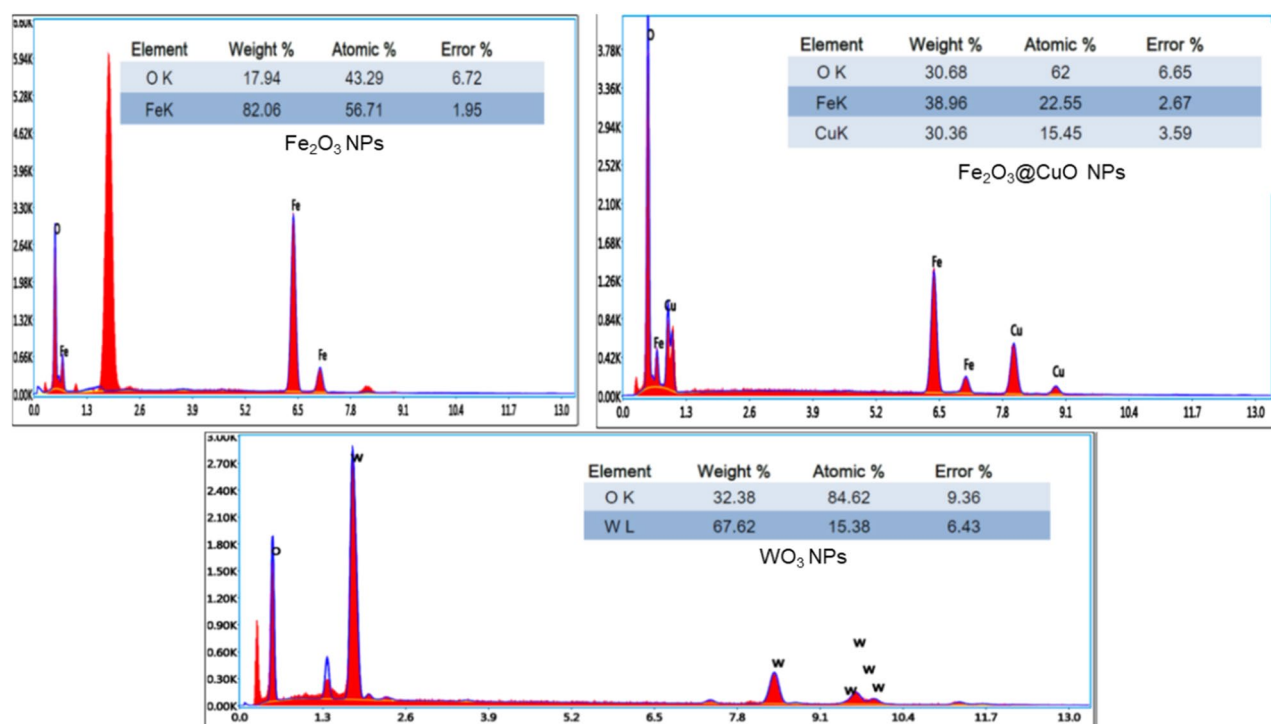

Figure 4. EDAX analysis of synthesized magnetic NPs of Fe_2O_3, Fe_2O_3@CuO and WO_3.

Fe₂O₃		Fe₂O₃@CuO		WO₃	
Element	Wight (%)	Element	Wight (%)	Element	Wight (%)
O	17.94	O	30.68	O	84.62
Fe	82.06	Fe	38.96	W	15.38
		Cu	30.36		
Total	100	Total	100	Total	100

Table 2. EDX results of the prepared NPs samples.

EDX analysis. These results are in good agreement with the crystal structures provided by XRD investigations (Figs. 1 and 2).

Biological activity evaluations

Antimicrobial activity

To evaluate the antimicrobial efficacy, synthesized Fe_2O_3, $Fe_2O_3@CuO$, and WO_3 NPs were studied individually against different human pathogens such as *E. coli, S. aureus,* and *C. Albicans*. A wide range of tested nanomaterial concentrations (10, 50, 90, 130, 170, 210, 250, and 290 mg/ml) were studied to find appropriate ranges for all examined nanoparticles. According to Fig. 5, the highest inhibition zones of $Fe_2O_3@CuO$ NPs and Fe_2O_3 NPs were observed at low concentrations that ranged from (10 to 50 mg/ml). Nevertheless, the largest concentrations of WO_3 NPs (90 to 250 mg/ml) produced the widest inhibition zones against all tested pathogens, as shown in (Fig. 5). Also, *C. Albicans* showed clear resistance nearly to all tested nanoparticles; whereas *Gram*-negative bacteria are affected perfectly, followed by *Gram*-positive bacteria.

Subsequently, the MICs for all tested nanoparticles were determined as shown in Table 3. The inhibition zones generated by applying different doses of $Fe_2O_3@CuO$, Fe_2O_3, and WO_3 NPs against all tested human pathogens are depicted in the antimicrobial photographs in Fig. 6. When compared to controls, all of the synthesized Fe_2O_3, $Fe_2O_3@CuO$, and WO_3 NPs exhibit significant antimicrobial effects against all tested human pathogens. It was clearly observed that the highest antibacterial potency was detected against *E. coli* (38.45 ± 3.12 mm) in case of WO_3 NPs at 250 mg/ml, followed by 20 mg/ml of Fe_2O_3 NPs (33.56 ± 3.25 mm). However, the lowest inhibition zone was determined in case of *E. coli* (22.67 ± 2.08 mm) at 40 mg/ml of $Fe_2O_3@CuO$ NPs (Table 3 and Fig. 7). However, in the case of *S. aureus*, the maximum antibacterial potency was recorded at 40 mg/ml of $Fe_2O_3@CuO$ NPS (32.86 ± 3.21 mm) and the lowest one was recorded at 100 mg/ml of WO_3NPs (19.36 ± 1.08 mm), as shown in (Fig. 7). This indicates that antimicrobial activity depends on both type of bacterial species and nanoparticles concentrations. Nevertheless, the resistance was relatively dominant for all tested nanoparticles ($Fe_2O_3@CuO$, Fe_2O_3, and WO_3 NPs) in the case of fungal cells (Table 3 and Fig. 7).

Recently, polymers modified with large-surface-area of NPs, such as Fe_2O_3, and WO_3 NPs have been employed for a variety of applications including drug release, tissue regeneration, heavy metal adsorption, cell separation, antimicrobial agents, and the treatment of malignant brain tumours and breast cancer cells[70,71]. They have low volume/surface area ratios, high adsorption capabilities, and selective target molecule adsorption[72]. While, another report has revealed that the charge potential of both the fabricated nanoparticles and the tested microbial cells influences antimicrobial properties. Furthermore, the Concentration, shape, and size of the nanoparticles generated have an impact on overall bioactivity, which are among the primary causes for NP attachment or non-attachment to microbial cells.
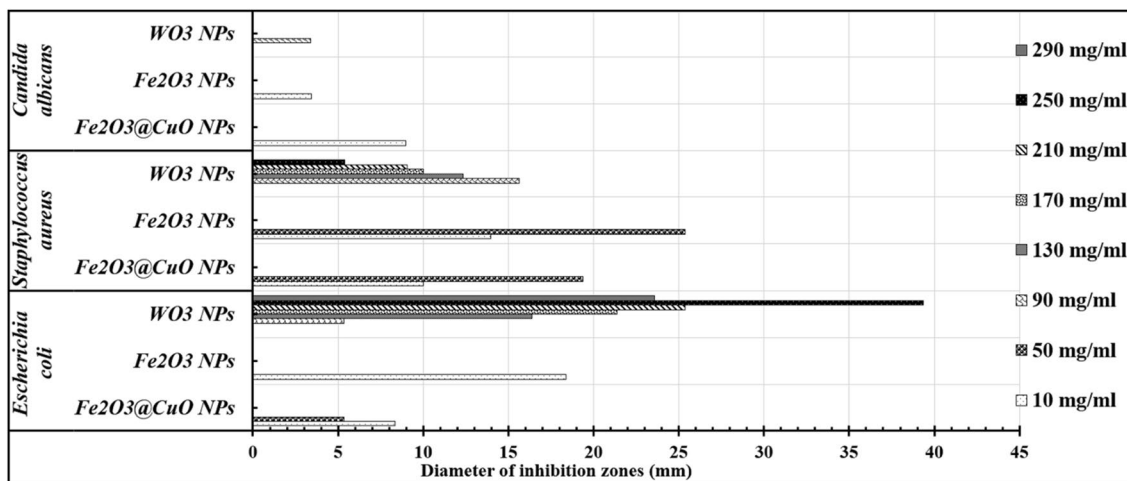

Figure 5. Survey of the inhibitory concentration ranges of $Fe_2O_3@CuO$ NPs, Fe_2O_3 NPs, and WO_3 NPs against some human pathogens including *E. coli*, *S. aureus*, and *C. albicans*.

Treatments	Concentrations	*Escherichia coli*	*Staphylococcus aureus*	*Candida albicans*
Controls	Ampicillin 10 mg	3.04 ± 0.02	2.54 ± 0.14	1.02 ± 0.98
	Penicillin 10 μg	0.96 ± 1.02	2.48 ± 0.39	1.45 ± 0.92
	Ciprofloxacin 5 μg	3.21 ± 1.98	1.69 ± 0.95	0.54 ± 0.95
Fe2O3@CuO NPs	10 mg/ml	7.3 ± 3.61	9.8 ± 4.63	9.36 ± 2.36
	20 mg/ml	14.26 ± 1.52	12.79 ± 4.56	0
	30 mg/ml	16 ± 3.65	19.67 ± 7.78	0
	40 mg/ml	22.67 ± 2.08	32.86 ± 3.21	0
Fe_2O_3 NPs	5 mg/ml	16.56 ± 1.53	8.56 ± 0.69	5.23 ± 0.59
	10 mg/ml	19.68 ± 4.04	14.36 ± 2.23	0
	15 mg/ml	27.3 ± 7.09	23.67 ± 1.36	0
	20 mg/ml	33.56 ± 3.25	27.58 ± 3.58	0
WO_3 NPs	100 mg/ml	6.56 ± 5.51	19.36 ± 1.08	3.56 ± 0.14
	150 mg/ml	19.36 ± 4.35	13.45 ± 0.96	0
	200 mg/ml	24.12 ± 3.06	10.36 ± 0.96	0
	250 mg/ml	38.45 ± 3.12	6.59 ± 0.89	0

Table 3. Antimicrobial activity of different concentrations of Fe_2O_3, Fe_2O_3@CuO and WO_3 NPs against varied human pathogens compared with different common antibiotics as controls.
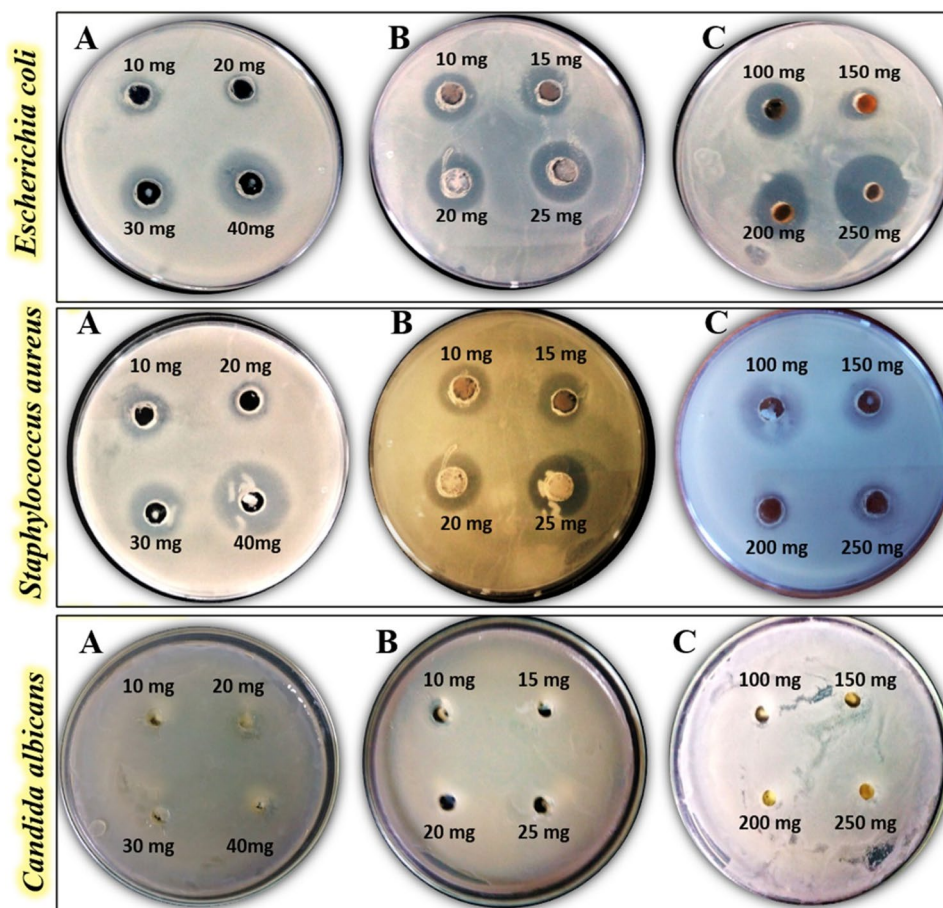

Figure 6. Antimicrobial activity of Fe_2O_3@CuO NPs (**A**); Fe_2O_3 NPs (**B**) and WO_3 NPs (**C**) against tested human pathogens.
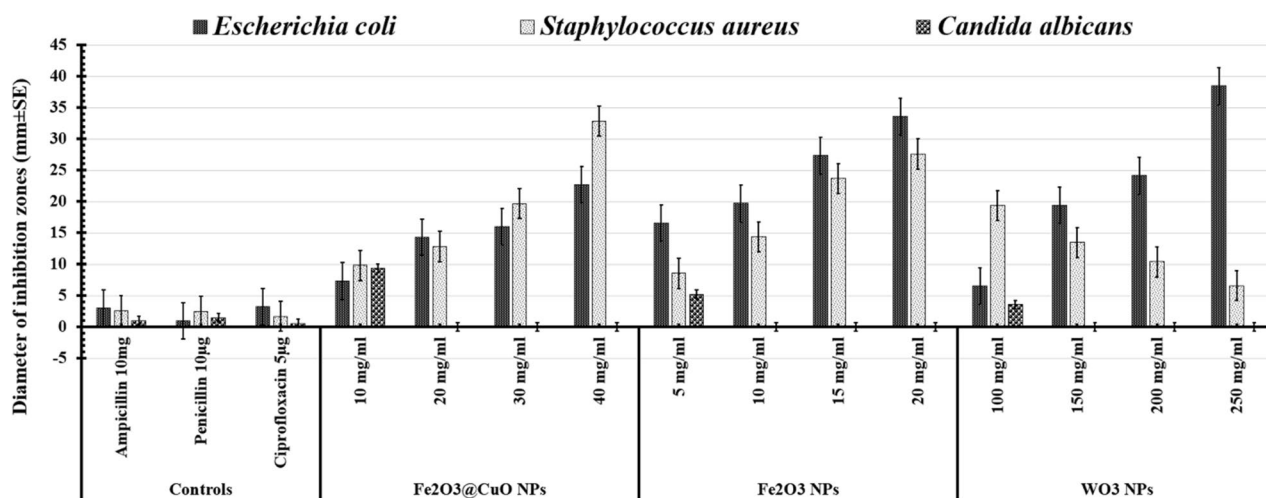
Figure 7. Antimicrobial activity of Fe$_2$O$_3$@CuO NPs (10 mg/ml**,** 20 mg/ml**,** 30 mg/ml, and 40 mg/ml)**;** Fe$_2$O$_3$ NPs (10 mg/ml, 15 mg/ml, 20 mg/ml, and 25 mg/ml), and WO$_3$ NPs (100 mg/ml**,** 150 mg/ml, 200 mg/ml, and 250 mg/ml) against different human pathogens compared to various conventional antibiotics as controls, including 5 μg of Ciprofloxacin, 10 μg of Penicillin, and 10 mg of Ampicillin.

According to Pekdemir et al.[73], Fe$_2$O$_3$NP-pathogen cell contact would be poor due to prevailing electrostatic repulsion at the interface, which is the underlying cause of the NP's non-attachment to the microbial cells. Moreover, at high concentrations of at least 50 μM (critical concentration); they observed some antimicrobial effects. Also, Borcherding et al.[74], reported excellent antimicrobial activities at different n-IONP dosages, which are consistent with our findings. Since increased n-IONP concentrations in the culture media might also promote the production of reactive oxygen species (ROS) (including superoxide radical, hydrogen peroxide, and hydroxyl radical), which is one of the key causes of metal oxide nanoparticles' antimicrobial properties[75,76]. Furthermore, physical contact between nanoparticles and microbial wall membranes modifies cell permeability, which subsequently leads to microbial mortality[77,78].

Cytotoxicity test
<u>MTT-assay.</u>   MTT colorimetric assay was performed on *Vero* and *MCF-7* cell lines with serial concentrations of each synthesized NPs, as shown in Fig. 8. After treatment with different concentrations of NPs, the results were obtained by calculation of IC50 value using *Graph Pad Prism software version 6*.

IC50 values were detected at concentrations of 40.24, 21.13, and 25.41 μg/ml for Fe$_2$O$_3$, Fe$_2$O$_3$@CuO, and WO$_3$NPs respectively on Vero cells, whereas on MCF-7 these values were detected at 12.87, 8.876 and 9.211 μg/ml; respectively for the same materials. Our tested NPs demonstrated anti-proliferative activity against replication of in vitro model of human breast cancer cells (MCF-7) (Fig. 8).

Furthermore, morphological examination of *MCF-7* cells revealed a distinctive change in the morphology of *MCF-7* cells from a healthy spindle-like shape to a rounded morphology, and cells were also observed to form small irregular aggregations due to the toxicity induced by magnetic NPs on them. Such toxicity is due to the production of reactive oxygen species (ROS)[19,37] DNA injury and fragmentation, lipid peroxidation and genotoxic effect through chromosomal damage[27]. Leading to caspase activation which push cancer cells apoptotic pathway[79] and cell death in response to the toxic effect of magnetic nanoparticles. These findings support the anti-cancer effects of the synthesized magnetic NPs[22,80].

Antiviral assay against human Adenovirus type-5(ADV-5) on Vero cells
Quantitative measurement of antiviral activity using real-time PCR against Adenovirus (ADV-5) was determined for our proposed materials using two mechanisms including virucidal and viral adsorption mechanisms. Results showed that all tested materials have antiviral activity via viral adsorption mechanism for both Fe$_2$O$_3$@CuO and WO$_3$ NPs as evidenced by the undetectable level of viral load (copies/mL) although, Fe$_2$O$_3$ NPs decreased the viral copies reach 80% reduction compared with the positive control. This indicates that the nanoparticles' effect was to prevent viruses' entry into host cells[61,81].

<u>Virucidal mechanism.</u>   Figure 9 represents a chart of viral adsorption mechanism. This mechanism depended on investigating viral titer through the ability of the tested nanoparticles to neutralize the virus and block its affinity to enter and infect the cells Therefore, lost its ability to replicate inside the cells[82] Results showed the synthesized Fe$_2$O$_3$, Fe$_2$O$_3$@CuO, and WO$_3$ NPs inhibited the viral titer as evidenced by this assay (Table 4). The viral titer was involved (copies/mL) as a result the tested materials showed high antiviral properties against *ADV*-5 and detected levels of viral copies using quantitative real-time PCR (Table 4). Fe$_2$O$_3$ treated infected cells gave viral titer (3.3×10^4) Copies/ml, Fe$_2$O$_3$@Cuo treated infected cells was (2×10^5 Copies/ml), WO3 treated infected cells was (8.5×10^4 Copies/ml), showing the reduction in viral titer as 99% reduction compared to viral control
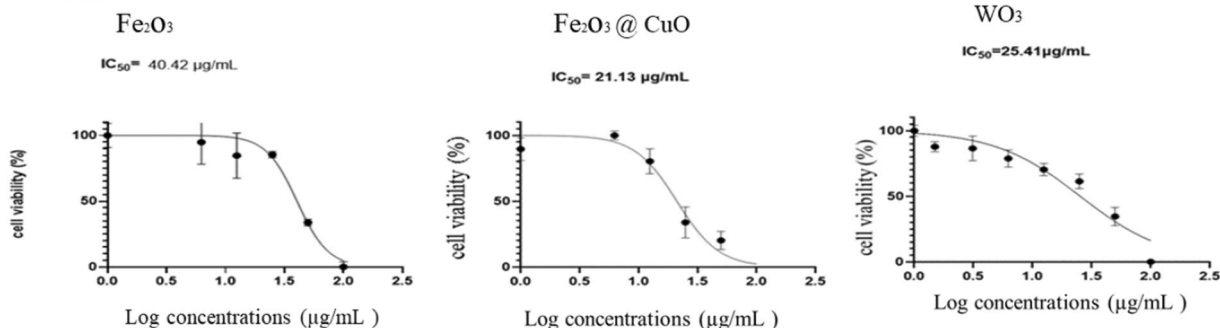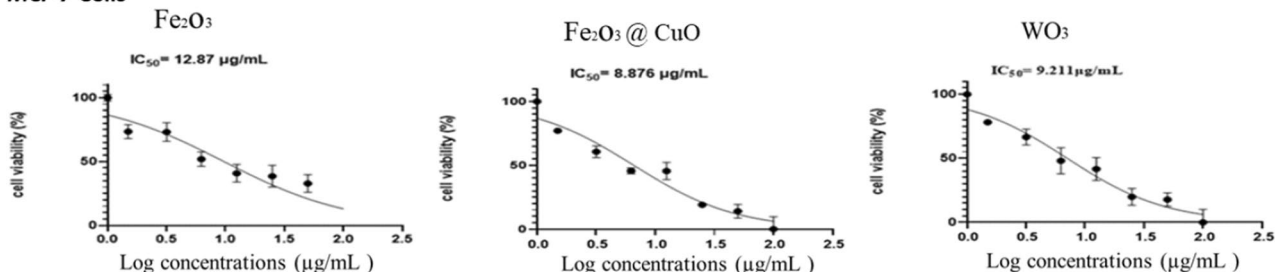
Figure 8. IC$_{50}$ charts through MTT-assay of synthesized Fe$_2$O$_3$, Fe$_2$O$_3$@CuO and WO$_3$ NPs with different concentrations using *Vero* (normal cell line) (up) and *MCF-7* (cancer cell line) (down).

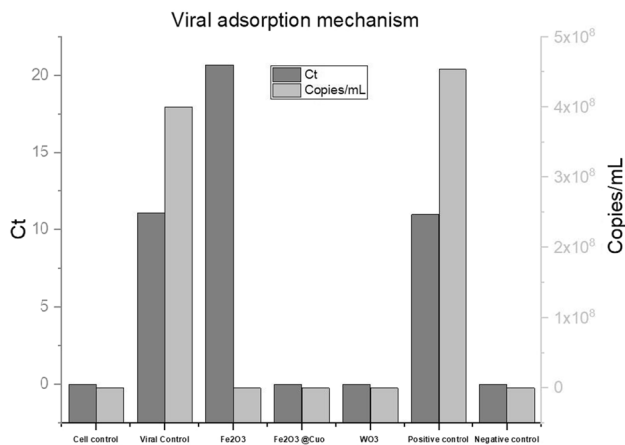**Figure 9.** Chart of viral adsorption mechanism represented against Adino virus.

AdV-5	CT	Copies/mL
Untreated *Vero* cells (cell control)	Under detection	Under detection
Positive cells infected with AdV5 (viral control)	11.08	4×10^8
Fe$_2$O$_3$-treated infected cells	19.16	3.3×10^4
Fe$_2$O$_3$@Cuo NPs treated infected cells	19.69	2.0×10^5
WO3-treated infected cells	20.71	8.5×10^4
Positive control	10.97	4.54×10^8
Negative control	Under detection	Under detection

Table 4. Real-time PCR assay of AdV-5 treated cells with synthesized MNPs using (virucidal mechanism).

AdV-5	CT	Copies/ml
Untreated Vero cells (cell control)	Under detection	Under detection
Positive cells infected with AdV5 (viral control)	11.08	4×10^8
Fe_2O_3 treated infected cells	20.68	8.8×10^4
Fe_2O_3 @Cuo treated infected cells	Under detection	Under detection
WO3-treated infected cells	Under detection	Under detection
Positive control	10.97	4.54×10^8
Negative control	Under detection	Under detection

Table 5. Real-time PCR assay of AdV-5 treated cells with synthesized MNPs using (Viral adsorption mechanism).

(4.54×10^8 Copies/ml). Consequently, this detailed study as virucidal and viral adsorption mechanisms of MNPs proved the high affinity of magnetic NPs as a potent antiviral agent[40].

<u>Viral adsorption mechanism.</u>   Concerning the antiviral adsorption mechanism this mechanism depended on the affinity of the tested materials to inhibit the viral entry, and replication and also prevent its spread to cells during its pathogenesis process, two materials were able to prevent viral replication inside the cells, thus demonstrating the antiviral activity without affecting cell viability (Table 5). The results demonstrated the potent of Fe_2O_3 as an antiviral inhibitor by decreasing the viral titer and rationalized their effect an equivalent reduction of viral titer reach to 99% compared to the positive control, the viral titer for Fe_2O_3 NPs was (8.8×10^4), compared to the positive control was 4.54×10^8 while Fe_2O_3@CuO and WO_3 NPs showed the great effect that the viral load was under detectable inside the treated cells. MNPs cause irreversible damage to the viral genome and inactivation of viral genome replication which prevents viral replication inside the treated cells. By another mechanism, MNPs block the viral entry into the cells, as evidenced by undetected viral copies by real-time PCR assay[83,61].

Conclusions
In conclusion, Fe_2O_3, Fe_2O_3@CuO, and WO_3 NPs were successfully synthesized, fully characterized, and structure evaluated; these materials were greatly applied in biomedical aspects due to their biocompatibility and chemical stability which play a great role as an antiproliferative effect against breast cancer, IC50 on MCF-7(human breast cancer) was detected at 12.87, 8.876, and 9.211 μg/ml for Fe_2O_3, Fe_2O_3@CuO, and WO_3 respectively. The combination of iron oxide with copper oxide improved the anti-proliferative activity of iron oxide and increased its toxicity against the replication of cancer cells. The result showed that iron oxide modified with copper oxide nanoparticles (Fe_2O_3@CuO NPs) demonstrated the highest anticancer activity against an in vitro model of human breast cancer cells affecting their morphological appearance and confirmed by low IC50 value. Fe_2O_3, Fe_2O_3@CuO, and WO_3 were observed against replication of human adenovirus type 5 as a respiratory viral model. Fe_2O_3@CuO and WO_3 gave a complete reduction of viral titer to an undetectable level, and Fe_2O_3 gave a reduction of more than 60% which proves the high potency of these tested materials against viral infection. In addition, their activity was demonstrated against gram-positive and gram-negative bacteria. In this study, we obtained a clear view of the potency of the tested MNPs as promising antiviral agents against ADV-5 (respiratory viral model). Therefore, our synthesized materials, Fe_2O_3, Fe_2O_3@CuO, and WO3 NPs, showed promising candidates and will be subjected to further insight and investigation on a molecular level to elucidate the interplay between apoptotic gene expression (programmed cell death) and their role in cancer death and in vivo studies before their application in clinical settings.

Data availability
The datasets used and/or analysed during the current study available from the corresponding author on reasonable request.

References
1. Ganapathe, L. S., Mohamed, M. A., Yunus, R. M. & Berhanuddin, D. D. Magnetite (Fe3O4) nanoparticles in biomedical application: from synthesis to surface functionalisation. *Magnetochemistry* **6**(4), 1–35. https://doi.org/10.3390/magnetochemistry6040068 (2020).
2. Sharmin, S. *et al.* Nanoparticles as antimicrobial and antiviral agents: A literature-based perspective study. *Heliyon* **7**(3), e06456. https://doi.org/10.1016/j.heliyon.2021.e06456 (2021).
3. Pourmadadi, M. *et al.* Role of iron oxide (Fe2O3) nanocomposites in advanced biomedical applications: A State-of-the-Art review. *Nanomaterials* **12**(21), 3873. https://doi.org/10.3390/nano12213873 (2022).
4. Gnanavel, V., Palanichamy, V. & Roopan, S. M. Biosynthesis and characterization of copper oxide nanoparticles and its anticancer activity on human colon cancer cell lines (HCT-116). *J. Photochem. Photobiol. B* **171**, 133–138. https://doi.org/10.1016/J.JPHOTOBIOL.2017.05.001 (2017).
5. Deepika, S., Selvaraj, C. I. & Roopan, S. M. Screening bioactivities of Caesalpinia pulcherrima L. swartz and cytotoxicity of extract synthesized silver nanoparticles on HCT116 cell line. *Mater. Sci. Eng. C* **106**, 110279. https://doi.org/10.1016/j.msec.2019.110279 (2020).
6. Clement, J. H. *et al.* Differential interaction of magnetic nanoparticles with tumor cells and peripheral blood cells. *J. Cancer. Res. Clin. Oncol.* **132**, 287–292. https://doi.org/10.1007/s00432-006-0076-x (2006).

7. Knežević, N., Gadjanski, I. & Durand, J. O. Magnetic nanoarchitectures for cancer sensing, imaging and therapy. *J. Mater. Chem. B* **7**(1), 9–23. https://doi.org/10.1039/c8tb02741b (2019).

8. Zhang, G. *et al.* Hydroxycamptothecin-loaded Fe3O4 nanoparticles induce human lung cancer cell apoptosis through caspase-8 pathway activation and disrupt tight junctions. *Cancer Sci.* **102**(6), 1216–1222. https://doi.org/10.1111/j.1349-7006.2011.01930.x (2011).

9. Jacob, J. A., Salmani, J. M. M. & Chen, B. Magnetic nanoparticles: Mechanistic studies on the cancer cell interaction. *Nanotechnol. Rev.* **5**(5), 481–488. https://doi.org/10.1515/ntrev-2016-0022 (2016).

10. Rajeshkumar, S., Malarkodi, C., Al Farraj, D. A., Soliman Elshikh, M. & Mohana Roopan, S. Employing sulphated polysaccharide (fucoidan) as medium for gold nanoparticles preparation and its anticancer study against HepG2 cell lines. *Mater. Today Commun.* **26**, 101975. https://doi.org/10.1016/j.mtcomm.2020.101975 (2021).

11. Wu, W., He, Q. & Jiang, C. Magnetic iron oxide nanoparticles: Synthesis and surface functionalization strategies. *Nanoscale Res. Lett.* **3**(11), 397–415. https://doi.org/10.1007/s11671-008-9174-9 (2008).

12. Merkl, P., Long, S., McInerney, G. M. & Sotiriou, G. A. Antiviral activity of silver, copper oxide and zinc oxide nanoparticle coatings against Sars-Cov-2. *Nanomaterials* **11**(5), 1312. https://doi.org/10.3390/nano11051312 (2021).

13. Shahabadi, N., Falsafi, M., Feizi, F. & Khodarahmi, R. Functionalization of γ-Fe2O3@SiO2 nanoparticles using the antiviral drug zidovudine: synthesis, characterization: In vitro cytotoxicity and DNA interaction studies. *RSC Adv.* **6**(77), 73605–73616. https://doi.org/10.1039/c6ra16564h (2016).

14. Fan, X. *et al.* Thermoresponsive supramolecular chemotherapy by "V"-shaped armed β-cyclodextrin star polymer to overcome drug resistance. *Adv. Healthc. Mater.* **7**(7), 1–11. https://doi.org/10.1002/adhm.201701143 (2018).

15. Pan, B. *et al.* Dendrimer-modified magnetic nanoparticles enhance efficiency of gene delivery system. *Cancer Res.* **67**(17), 8156–8163. https://doi.org/10.1158/0008-5472.CAN-06-4762 (2007).

16. Shao, H., Yoon, T. J., Liong, M., Weissleder, R. & Lee, H. Magnetic nanoparticles for biomedical NMR-based diagnostics. *Beilstein J. Nanotechnol.* **1**(1), 142–154. https://doi.org/10.3762/bjnano.1.17 (2010).

17. Jat, S. K., Gandhi, H. A., Bhattacharya, J. & Sharma, M. K. Magnetic nanoparticles: An emerging nano-based tool to fight against viral infections. *Mater. Adv.* **2**(14), 4479–4496. https://doi.org/10.1039/d1ma00240f (2021).

18. Gupta, A. K. & Curtis, A. S. G. Surface modified superparamagnetic nanoparticles for drug delivery: Interaction studies with human fibroblasts in culture. *J. Mater. Sci. Mater. Med.* **15**(4), 493–496. https://doi.org/10.1023/B:JMSM.0000021126.32934.20 (2004).

19. Ahamed, M., Alhadlaq, H. A., Khan, M. A. M. & Akhtar, M. J. Selective killing of cancer cells by iron oxide nanoparticles mediated through reactive oxygen species via P53 pathway. *J. Nanopart. Res.* **15**(1), 1225. https://doi.org/10.1007/s11051-012-1225-6 (2013).

20. Rajeshkumar, S. *et al.* Biosynthesis of zinc oxide nanoparticles using *Mangifera indica* leaves and evaluation of their antioxidant and cytotoxic properties in lung cancer (A549) cells. *Enzyme Microb. Technol.* **117**, 91–95. https://doi.org/10.1016/j.enzmictec.2018.06.009 (2018).

21. Alangari, A. *et al.* Iron oxide nanoparticles: Preparation, characterization, and assessment of antimicrobial and anticancer activity. *Adsorpt. Sci. Technol.* **2022**, 1–9. https://doi.org/10.1155/2022/1562051 (2022).

22. Yoonus, J., Resmi, R. & Beena, B. Evaluation of antibacterial and anticancer activity of green synthesized iron oxide (α-Fe2O3) nanoparticles. *Mater. Today Proc.* **46**, 2969–2974. https://doi.org/10.1016/J.MATPR.2020.12.426 (2021).

23. Profile, S. E. E. Potential nanomaterials and their applications in modern medicine: An overview. *ARC J. Cancer Sci.* https://doi.org/10.20431/2455-6009.0202004 (2016).

24. Cagno, V. *et al.* Broad-spectrum non-toxic antiviral nanoparticles with a virucidal inhibition mechanism. *Nat. Mater.* **17**(2), 195–203. https://doi.org/10.1038/NMAT5053 (2018).

25. Cao, Y. *et al.* Green synthesis of bimetallic ZnO–CuO nanoparticles and their cytotoxicity properties. *Sci. Rep.* **11**(1), 1–8. https://doi.org/10.1038/s41598-021-02937-1 (2021).

26. Jeronsia, J. E., Vidhya Raj, D. J., Joseph, L. A., Rubini, K. & Das, S. J. In vitro antibacterial and anticancer activity of copper oxide nanostructures in human breast cancer Michigan cancer foundation-7 cells. *J. Med. Sci. (Taiwan)* **36**(4), 145–151. https://doi.org/10.4103/1011-4564.188899 (2016).

27. Siddiqui, M. A. *et al.* Copper oxide nanoparticles induced mitochondria mediated apoptosis in human hepatocarcinoma cells. *PLoS ONE* **8**(8), 69354. https://doi.org/10.1371/journal.pone.0069534 (2013).

28. Navada, K. M. *et al.* Synthesis, characterization of phyto-functionalized CuO nano photocatalysts for mitigation of textile dyes in waste water purification, antioxidant anti-inflammatory and anticancer evaluation. *Appl. Nanosci.* **11**(4), 1313–1338. https://doi.org/10.1007/s13204-021-01688-9 (2021).

29. Sankar, R., Maheswari, R., Karthik, S., Shivashangari, K. S. & Ravikumar, V. Anticancer activity of ficus religiosa engineered copper oxide nanoparticles. *Mater. Sci. Eng. C* **44**, 234–239. https://doi.org/10.1016/j.msec.2014.08.030 (2008).

30. Kalaiarasi, A. *et al.* Copper oxide nanoparticles induce anticancer activity in A549 lung cancer cells by inhibition of histone deacetylase. *Biotechnol. Lett.* **40**(2), 249–256. https://doi.org/10.1007/s10529-017-2463-6 (2018).

31. Elemike, E. E., Onwudiwe, D. C. & Singh, M. Eco-friendly synthesis of copper oxide, zinc oxide and copper oxide-zinc oxide nanocomposites, and their anticancer applications. *J. Inorg. Organomet. Polym. Mater.* **30**(2), 400–409. https://doi.org/10.1007/s10904-019-01198-w (2020).

32. Abu-Serie, M. M. & Eltarahony, M. Novel nanoformulation of disulfiram with bacterially synthesized copper oxide nanoparticles for augmenting anticancer activity: An in vitro study. *Cancer Nanotechnol.* **12**(1), 25. https://doi.org/10.1186/s12645-021-00097-5 (2021).

33. Nagajyothi, P. C., Muthuraman, P., Sreekanth, T. V. M., Kim, D. H. & Shim, J. Green Synthesis: In-Vitro Anticancer Activity of Copper Oxide Nanoparticles against Human Cervical Carcinoma Cells. *Arabian Journal of Chemistry* **10**(2), 215–225. https://doi.org/10.1016/j.arabjc.2016.01.011 (2017).

34. Rajamma, R., Nair, S. G., Khadar, F. A. & Baskaran, B. Antibacterial and anticancer activity of biosynthesised CuO nanoparticles. *IET Nanobiotechnol.* **14**(9), 833–838. https://doi.org/10.1049/iet-nbt.2020.0088 (2020).

35. Matharu, R. K., Ciric, L., Ren, G. & Edirisinghe, M. Comparative study of the antimicrobial effects of tungsten nanoparticles and tungsten nanocomposite fibres on hospital acquired bacterial and viral pathogens. *Nanomaterials* **10**(6), 1017. https://doi.org/10.3390/nano10061017 (2020).

36. Brenneisen, P. & Reichert, A. S. Nanotherapy and reactive oxygen species (ROS) in cancer: A novel perspective. *Antioxidants* **7**(2), 31. https://doi.org/10.3390/antiox7020031 (2018).

37. Liman, R., Başbuğ, B., Muddassir Ali, M., Acikbas, Y. & HakkıCiğerci, İ. Cytotoxic and genotoxic assessment of tungsten oxide nanoparticles in allium cepa cells by allium ana-telophase and comet assays. *J. Appl. Genet.* **62**, 85–92. https://doi.org/10.1007/s13353-020-00608-x/Published (2021).

38. Sharma, A. *et al.* Methods of preparation of metal-doped and hybrid tungsten oxide nanoparticles for anticancer, antibacterial, and biosensing applications. *Surf. Interfaces* **2022**(28), 101641. https://doi.org/10.1016/j.surfin.2021.101641 (2021).

39. Sharma, A. *et al.* Methods of preparation of metal-doped and hybrid tungsten oxide nanoparticles for anticancer, antibacterial, and biosensing applications. *Surf. Interfaces* **28**, 101641. https://doi.org/10.1016/j.surfin.2021.101641 (2022).

40. Matsumoto, T. *et al.* Effects of cerium and tungsten substitution on antiviral and antibacterial properties of lanthanum molybdate. *Mater. Sci. Eng. C* **117**, 111323. https://doi.org/10.1016/J.MSEC.2020.111323 (2020).

41. Matsumoto, T. *et al.* Effects of cerium and tungsten substitution on antiviral and antibacterial properties of lanthanum molybdate. *Mater. Sci. Eng. C* **117**(August), 111323. https://doi.org/10.1016/j.msec.2020.111323 (2020).

42. Pfaff, F. *et al.* Tungsten carbide nanoparticles show a broad spectrum virucidal activity against enveloped and nonenveloped model viruses using a guideline-standardized in vitro test. *Lett. Appl. Microbiol.* **69**(4), 302–309. https://doi.org/10.1111/lam.13208 (2019).

43. Ghezzi, S. *et al.* Rapid inactivation of SARS-CoV-2 by coupling tungsten trioxide (WO3) photocatalyst with copper nanoclusters. *J. Nanotechnol. Nanomater.* **1**(3), 109–115. https://doi.org/10.33696/nanotechnol.1.014 (2020).

44. Carvalho, A. P. A. & Conte-Junior, C. A. Recent advances on nanomaterials to COVID-19 management: A systematic review on antiviral/virucidal agents and mechanisms of SARS-CoV-2 inhibition/inactivation. *Glob. Chall.* **5**(5), 2000115. https://doi.org/10.1002/gch2.202000115 (2021).

45. Elnouby, M. *et al.* Facile synthesis of WO3·H2O square nanoplates via a mild aging of ion-exchanged precursor. *J. Ceram. Soc. Jpn.* **121**(1418), 907–911. https://doi.org/10.2109/JCERSJ2.121.907 (2013).

46. Abed, M. *et al.* Synthesis of Ag/Au (Core/Shell) nanoparticles by laser ablation in liquid and study of their toxicity on blood human components. *J. Phys.* https://doi.org/10.1088/1742-6596/1795/1/012013 (2021).

47. Rashid, T. M., Nayef, U. M., Jabir, M. S. & Mutlak, F. A. H. Synthesis and characterization of Au:ZnO (Core:Shell) nanoparticles via laser ablation. *Optik* **244**, 167569. https://doi.org/10.1016/J.IJLEO.2021.167569 (2021).

48. Bakhshi, O., Bagherzade, G. & Ghamari Kargar, P. Biosynthesis of organic nanocomposite using Pistacia Vera L. Hull: An efficient antimicrobial agent. *Bioinorg. Chem. Appl.* https://doi.org/10.1155/2021/4105853 (2021).

49. Sreenivasa, N. *et al.* Biogenic synthesis of silver nanoparticles using *Paenibacillus* sp. in-vitro and their antibacterial, anticancer activity assessment against human colon tumour cell line. *J. Environ. Biol.* **42**(1), 118–127. https://doi.org/10.22438/JEB/42/1/MRN-1401 (2021).

50. Zhao, L., Gong, K., Wang, Y. & Kong, S. Rapid and environment-friendly preparation of silver nanoparticles and their inhibition against phytopathogenic fungi. *Micro Nano Lett.* **16**(3), 213–220. https://doi.org/10.1049/MNA2.12027 (2021).

51. Jabir, M. S. *et al.* Porous silicon nanoparticles prepared via an improved method: A developing strategy for a successful antimicrobial agent against *Escherichia coli* and *Staphylococcus aureus*. *IOP Conf. Ser. Mater. Sci. Eng.* **454**(1), 012077. https://doi.org/10.1088/1757-899X/454/1/012077 (2018).

52. Jabir, M. S. *et al.* Inhibition of *Staphylococcus aureus* α-hemolysin production using nanocurcumin capped Au@ZnO nanocomposite. *Bioinorg. Chem. Appl.* https://doi.org/10.1155/2022/2663812 (2022).

53. Hussain, A. *et al.* Biogenesis of ZnO nanoparticles using: Pandanus odorifer leaf extract: Anticancer and antimicrobial activities. *RSC Adv.* **9**(27), 15357–15369. https://doi.org/10.1039/c9ra01659g (2019).

54. Emam, A. N., Loutfy, S. A., Mostafa, A. A., Awad, H. & Mohamed, M. B. Cyto-toxicity, biocompatibility and cellular response of carbon dots-plasmonic based nano-hybrids for bioimaging. *RSC Adv.* **7**(38), 23502–23514. https://doi.org/10.1039/c7ra01423f (2017).

55. Ibrahim, A. A. *et al.* Pt(II)-thiocarbohydrazone complex as cytotoxic agent and apoptosis inducer in Caov-3 and HT-29 cells through the P53 and Caspase-8 pathways. *Pharmaceuticals* **14**(6), 509. https://doi.org/10.3390/PH14060509 (2021).

56. Yuan, Y. *et al.* In vitro cytotoxicity and induction of apoptosis by silica nanoparticles in human HepG2 hepatoma cells. *Int. J. Nanomed.* https://doi.org/10.2147/ijn.s24005 (2011).

57. Xue, Y. *et al.* Cytotoxicity and apoptosis induced by silver nanoparticles in human liver HepG2 cells in different dispersion media. *J. Appl. Toxicol.* **36**(3), 352–360. https://doi.org/10.1002/jat.3199 (2016).

58. Abaza, A. *et al.* Cytotoxic effect of chitosan based nanocomposite synthesized by radiation: In vitro liver and breast cancer cell line. *J. Pharm. Pharmacol.* **6**(4), 305–319. https://doi.org/10.17265/2328-2150/2018.04.002 (2018).

59. Faral-Tello, P. *et al.* Cytotoxic, virucidal, and antiviral activity of South American plant and algae extracts. *Sci. World J.* https://doi.org/10.1100/2012/174837 (2012).

60. Nageh, H. *et al.* Zinc oxide nanoparticle-loaded electrospun polyvinylidene fluoride nano fibers as a potential face protector against respiratory viral infections. *ACS Omega* https://doi.org/10.1021/acsomega.2c00458 (2022).

61. Kumar, R. *et al.* Iron oxide nanoparticles based antiviral activity of H1N1 Influenza A virus. *J. Infect. Chemother.* **25**(5), 325–329. https://doi.org/10.1016/j.jiac.2018.12.006 (2019).

62. Loutfy, S. A. *et al.* Antiviral activity of chitosan nanoparticles encapsulating curcumin against hepatitis C virus genotype 4a in human hepatoma cell lines. *Int. J. Nanomed.* **15**, 2699–2715. https://doi.org/10.2147/IJN.S241702 (2020).

63. Hartig, T. *et al.* ICVD polymer thin film bio-interface-performance for fibroblasts, cancer-cells, and viruses connected to their functional groups and in silico studies. *Adv. Mater. Interfaces* **11**, 2300587. https://doi.org/10.1002/ADMI.202300587 (2023).

64. Vecitis, C. D. Antiviral-nanoparticle interactions and reactions. *Environ. Sci. Nano* **8**(1), 11–19. https://doi.org/10.1039/d0en00980f (2021).

65. Osminkina, L. A. *et al.* Antiviral adsorption activity of porous silicon nanoparticles against different pathogenic human viruses. *Bioact. Mater.* **7**, 39–46. https://doi.org/10.1016/j.bioactmat.2021.06.001 (2022).

66. Soliman, H. M. A., Kashyout, A. B., el Nouby, M. S. & Abosehly, A. M. Preparation and characterizations of tungsten oxide electrochromic nanomaterials. *J. Mater. Sci. Mater. Electron.* **21**(12), 1313–1321. https://doi.org/10.1007/S10854-010-0068-0/TABLES/4 (2010).

67. Elsayed, E. M., Elnouby, M. S., Gouda, S. M. H., Elessawy, N. A. & Santos, D. M. F. Effect of the morphology of tungsten oxide embedded in sodium alginate/polyvinylpyrrolidone composite beads on the photocatalytic degradation of methylene blue dye solution. *Materials* **13**(8), 1905. https://doi.org/10.3390/MA13081905 (2020).

68. Silva, C. A. S. *et al.* Magnetic solid-phase microextraction for lead detection in aqueous samples using magnetite nanoparticles. *J. Braz. Chem. Soc.* **31**(1), 109–115. https://doi.org/10.21577/0103-5053.20190134 (2020).

69. Raul, P. K. *et al.* CuO nanorods: A potential and efficient adsorbent in water purification. *RSC Adv.* **4**(76), 40580–40587. https://doi.org/10.1039/C4RA04619F (2014).

70. Duan, G. *et al.* Robust antibacterial activity of tungsten oxide (WO3-x) nanodots. *Chem. Res. Toxicol.* **32**(7), 1357–1366. https://doi.org/10.1021/ACS.CHEMRESTOX.8B00399/SUPPL_FILE/TX8B00399_SI_001.PDF (2019).

71. Teow, S.-Y. *et al.* bactericidal properties of plants-derived metal and metal oxide nanoparticles (NPs). *Molecules* **23**(6), 1366. https://doi.org/10.3390/MOLECULES23061366 (2018).

72. Masjedi, A., Askarizadeh, E. & Baniyaghoob, S. Magnetic nanoparticles surface-modified with tridentate ligands for removal of heavy metal ions from water. *Mater. Chem. Phys.* **249**, 122917. https://doi.org/10.1016/J.MATCHEMPHYS.2020.122917 (2020).

73. Pekdemir, M. E., Pekdemir, S., İnci, Ş, Kırbağ, S. & Çiftci, M. Thermal, magnetic properties and antimicrobial effects of magnetic iron oxide nanoparticles treated with polygonum cognatum. *Iran J. Sci. Technol. Trans. A Sci.* **45**(5), 1579–1586. https://doi.org/10.1007/S40995-021-01167-4 (2021).

74. Borcherding, J. *et al.* Iron oxide nanoparticles induce *Pseudomonas aeruginosa* growth, induce biofilm formation, and inhibit antimicrobial peptide function. *Environ. Sci. Nano* **1**(2), 123–132. https://doi.org/10.1039/C3EN00029J (2014).

75. Gudkov, S. V. *et al.* Do iron oxide nanoparticles have significant antibacterial properties?. *Antibiotics* **10**(7), 884. https://doi.org/10.3390/ANTIBIOTICS10070884 (2021).

76. Arakha, M. *et al.* Antimicrobial activity of iron oxide nanoparticle upon modulation of nanoparticle-bacteria interface. *Sci. Rep.* **5**(1), 1–12. https://doi.org/10.1038/srep14813 (2015).

77. Baazeem, A. *et al.* In vitro antibacterial, antifungal, nematocidal and growth promoting activities of Trichoderma hamatum FB10 and its secondary metabolites. *J. Fungi* **7**(5), 331. https://doi.org/10.3390/JOF7050331 (2021).

78. Tiwari, V. *et al.* Mechanism of anti-bacterial activity of zinc oxide nanoparticle against carbapenem-resistant Acinetobacter baumannii. *Front. Microbiol.* **9**, 1218. https://doi.org/10.3389/FMICB.2018.01218/BIBTEX (2018).
79. Roopan, S. M., Kumar, S. H. S., Madhumitha, G. & Suthindhiran, K. Biogenic-production of SnO2 nanoparticles and its cytotoxic effect against hepatocellular carcinoma cell line (HepG2). *Appl. Biochem. Biotechnol.* **175**(3), 1567–1575. https://doi.org/10.1007/s12010-014-1381-5 (2015).
80. Lin, C. A. O. *et al.* Anti-tumor activity of self-charged (Eu, Ca): WO3 and Eu : CaWO4. *Nanoparticles* **35**(5), 767–772 (2012).
81. Gurunathan, S. *et al.* Antiviral potential of nanoparticles-can nanoparticles fight against coronaviruses?. *Nanomaterials* https://doi.org/10.3390/nano10091645 (2020).
82. Rakowska, P. D. *et al.* Antiviral surfaces and coatings and their mechanisms of action. *Commun. Mater.* **2**(1), 153. https://doi.org/10.1038/s43246-021-00153-y (2021).
83. Nayak, D. P. Virus morphology, replication, and assembly. *Viral Ecol.* https://doi.org/10.1016/B978-012362675-2/50004-5 (2000).

Acknowledgements

Author contributions

All authors have contributed to writing the main manuscript, A.T. prepared the figures, and data analysis and contributed to the main manuscript preparation. S.H.E. has conducted and written the part of bio-evaluation tests. M.E. has prepared and written the part of the NPS synthesis. R.A.H., M.F. and M.O.: Methodology, data analysis and chemicals donation. while E.A.K. and S.L. reviewed the final manuscript. All authors declare that the Journal has the author's permission to publish research findings.

Competing interests

The authors declare no competing interests.

Additional information

Supplementary Information The online version contains supplementary material available at https://doi.org/10.1038/s41598-024-55319-8.

Correspondence and requests for materials should be addressed to E.A.K. or M.E.

Reprints and permissions information is available at www.nature.com/reprints.

Publisher's note Springer Nature remains neutral with regard to jurisdictional claims in published maps and institutional affiliations.